Supporting Information for Ultra-low Surface Recombination Velocity in InP Nanowires Probed by Terahertz Spectroscopy

Hannah J. Joyce,*,† Jennifer Wong-Leung,‡ Chaw-Keong Yong,† Callum J. Docherty,† Suriati Paiman,‡,¶ Qiang Gao,‡ H. Hoe Tan,‡ Chennupati Jagadish,‡ James Lloyd-Hughes,† Laura M. Herz,† and Michael B. Johnston*,†

Clarendon Laboratory, Department of Physics, University of Oxford, Oxford, OX1 3PU, UK, Department of Electronic Materials Engineering, Research School of Physics and Engineering, Australian National University, Canberra, ACT 0200, Australia, and Department of Physics, Faculty of Science, Universiti Putra Malaysia, 43400 Serdang, Selangor, Malaysia

E-mail: h.joyce1@physics.ox.ac.uk; m.johnston1@physics.ox.ac.uk

Experimental details

Growth

InP (111)B substrates were treated with poly-L-lysine. The substrate was cleaved into four portions and to each portion colloidal Au nanoparticles of a particular diameter (20, 30, 50 or 80 nm) were applied. Nanowires were grown at a pressure of 100 mbar and a total gas flow rate of 15 slm.

*To whom correspondence should be addressed

†Clarendon Laboratory, Department of Physics, University of Oxford, Oxford, OX1 3PU, UK

‡Department of Electronic Materials Engineering, Research School of Physics and Engineering, Australian National University, Canberra, ACT 0200, Australia

¶Department of Physics, Faculty of Science, Universiti Putra Malaysia, 43400 Serdang, Selangor, Malaysia

Growth was performed at 420°C for 20 minutes using trimethylindium and phosphine precursors with a V/III ratio of 700.

Electron microscopy and calculation of average nanowire diameters

Field emission scanning electron microscopy (FESEM) was carried out using a Hitachi S4300 FESEM at an accelerating voltage of 5 kV.

FESEM images of nanowires of quartz were used to quantify the nanowire diameter distributions of each of the four samples. For each sample, at least 50 individual nanowires were examined. For each individual nanowire, measurements of nanowire diameter were taken at approximately 250 nm intervals along the entire nanowire length. Using these data an average diameter was calculated for each nanowire. Each nanowire was binned according to its average diameter. The histograms were constructed by plotting the percentage of nanowires in each bin. The total nanowire length was also measured for each nanowire. The average diameter, $\bar{d}$, for each sample (namely 50 nm, 85 nm, 135 nm and 160 nm) was then calculated using the formula:

$$\bar{d} = \frac{\sum d_i l_i}{\sum l_i} \tag{S.1}$$

where d_i is the average diameter of nanowire i and l_i is its length.

For transmission electron microscopy (TEM) investigations, nanowires were first mechanically transferred to holey carbon grids. TEM was performed using a Phillips CM300 TEM operated at 300 kV. At least 5 nanowires were examined from each sample. Nanowires were examined for crystal structure and stacking faults over their entire length.

Terahertz time-domain spectroscopy

An amplified Ti:Sapphire laser with 4 W average power was used to generate 35 fs pulses centred at 800 nm at a 5 kHz repetition rate. Each pulse was split into three paths: approximately 590 μJ/pulse was used as the optical pump to photoexcite the sample, 200 μJ/pulse was used to generate the THz

probe pulse via optical rectification in a 2 mm GaP crystal, and 1.6 μJ/pulse was used as a gate for electro-optic detection of the transmitted THz pulse with a 200 μm GaP crystal. The optical pump beam was attenuated using neutral density filters to produce sample photoexcitation fluences between 1 and 160 μJ/cm^2. At the sample, the optical pump beamwidth had a full width at half maximum (FWHM) of 13 mm, whereas the THz probe FWHM was only 1.3 mm. Therefore the terahertz probe measured an area of approximately constant photoexcited carrier density. The THz electric field, E, was detected using a balanced photodiode circuit, and the signal was extracted using a lock-in amplifier referenced to a 2.5 kHz chopper in the THz generation beam. A second lock-in amplifier was used to detect the optical pump-induced change in terahertz electric field, ΔE, by referencing to a 125 Hz chopper in the optical pump beam. Varying the delay between the optical pump, terahertz probe and optical gate pulse produced a two-dimensional map of the THz spectral response of the material as a function of time after photoexcitation. The measurements were performed at room temperature with the entire terahertz beam path under vacuum, to avoid absorption of the terahertz radiation by atmospheric water vapour.

Photoluminescence up-conversion spectroscopy

The samples were excited at 736 nm using a mode-locked Ti:Sapphire laser oscillator supplying 100 fs pulses at a 82 MHz repetition rate. The spectral resolution of the time-resolved PL system at the selected detection wavelengths was 32 meV with a time-resolution of 200 fs. The PL was gated optically in a β-barium borate crystal using a fraction of the laser output that was subjected to an adjustable time delay with respect to the excitation pulse. Time-resolved PL measurements were recorded with a liquid-nitrogen cooled charge-coupled device (CCD) detector connected to a spectrometer.

Contribution of nanowire top and base to total surface area

We approximate the nanowire shape as a truncated cone with height, h, top diameter d_{top} and tapering angle, θ, as illustrated in Figure S.1a. The top surface area is given by

$$\pi r_{\text{top}}^2, \tag{S.2}$$

where $r_{\text{top}} = \frac{1}{2} d_{\text{top}}$. The bottom surface area is given by

$$\pi \left(r_{\text{top}} + h \tan\theta \right)^2. \tag{S.3}$$

The surface area made up by the lateral side surfaces is given by

$$\frac{\pi h}{\cos\theta} \left(2 r_{\text{top}} + h \tan\theta \right). \tag{S.4}$$

The summation of these three terms, S.2 to S.4, gives the total surface area. The sum of terms S.2 and S.3 gives the contribution of the top and bottom faces to the total surface area. Figure S.1b plots the proportion of the total surface area due to the sum of the top and bottom surfaces, as a function of nanowire aspect ratio, h/d_{top}. The data for four different tapering angles, θ, were plotted. The tapering angle $\theta = 0$ corresponds to an untapered cylinder. The remaining three tapering angles are typical of the nanowires of our study. The range of aspect ratios plotted is also typical of the nanowires of our study. It is clear from Figure S.1b that the top and bottom surfaces make only a small contribution to the total surface area, whereas the lateral side surfaces make the dominant contribution to total nanowire surface area. We therefore we may neglect the top and bottom surfaces in our analysis, and focus on the dependence of carrier lifetime as a function of nanowire diameter.

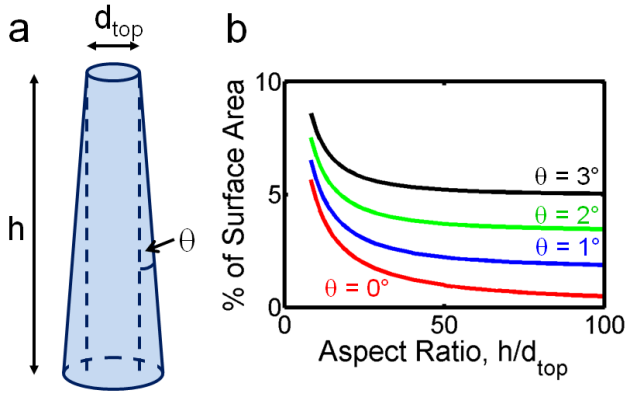

Figure S.1: (a) Schematic of a truncated cone, illustrating the parameters defining the nanowire shape: height, h, top diameter, d_{top}, and tapering angle, θ. (b) Plot of the contribution made by the sum of nanowire top surface and base surface to the total surface area.

Calculation of surface recombination velocity

To calculate the surface recombination velocity, we have followed the methods derived by Léonard *et al.* and Dan *et al.*[1,2] The nanowire geometry is approximated as a cylinder of infinite length, for which the continuity equation describing the carrier concentration profile is given by

$$\frac{\partial(\Delta n)}{\partial t} = D\frac{\partial^2(\Delta n)}{\partial r^2} - \frac{\Delta n}{\tau_{\text{volume}}}, \tag{S.5}$$

where Δn is the photoexcited electron density, D is the diffusion constant, r is the radial coordinate and τ_{volume} is the electron lifetime in bulk InP. This continuity equation is subject to the boundary conditions:

$$D\frac{\partial(\Delta n)}{\partial r}|_{r=\frac{d}{2}} = -S\Delta n, \tag{S.6}$$

where d is the nanowire diameter and S is the surface recombination velocity. Solution of the continuity equation gives an exponential time decay of the carrier density with the following expression for carrier lifetime:

$$\frac{1}{\tau} = \frac{1}{\tau_{\text{volume}}} + \frac{4\beta^2 D}{d^2}, \tag{S.7}$$

In the above equation, β is given by

$$\beta J_1(\beta) - L J_0(\beta) = 0, \tag{S.8}$$

where J_0 and J_1 are 0^{th} and 1^{st} order Bessel functions of the first kind and

$$L = \frac{dS}{2D}. \tag{S.9}$$

For small β we can use the small argument behaviour of Bessel functions:

$$J_n(\beta) \approx \frac{1}{2^n n!}\beta^n, \tag{S.10}$$

so that $J_0(\beta) = 1$ and $J_1(\beta) = \frac{1}{2}\beta$. Substituting these values into Equation (S.8) gives $\beta = \sqrt{2L}$. Using this approximation, Equation (S.7) simplifies to

$$\frac{1}{\tau} = \frac{1}{\tau_{\text{volume}}} + \frac{4S}{d}. \tag{S.11}$$

Equation (S.11) was then fitted to the monoexponential decay lifetimes ($\tau = 1.18$ ns, 1.27 ns, 1.30 ns and 1.34 ns) of the four samples ($d = 50$, 85, 135 and 160 nm, respectively), as plotted in Figure S.2. This yielded τ_{volume} of 1.4 ns and a surface recombination velocity of 170 cm/s.

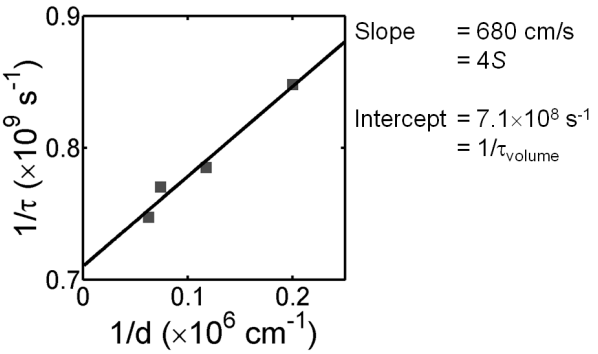

Figure S.2: Plot of decay rate, $\frac{1}{\tau}$, against inverse nanowire diameter, $\frac{1}{d}$. This plot was used to extract the surface recombination velocity, S, and bulk recombination lifetime, τ_{volume}. Square symbols represent the monoexponential decay lifetimes for the four samples of different diameter. The black line is the line of best fit to Equation (S.11).

To confirm that the initial approximation of small β is valid, we verify that $L = \frac{dS}{2D} \ll 1$, as follows. The minimum diffusion constant is calculated using the Einstein relation and inserting the lowest measured mobility of $120\,\mathrm{cm^2V^{-1}s^{-1}}$:

$$D = \frac{\mu k_\mathrm{B} T}{e} = 3.1\,\mathrm{cm^2 s^{-1}}. \tag{S.12}$$

The maximum nanowire diameter is 160 nm and $S = 170$ cm/s. Therefore $L = \frac{dS}{2D} < 4.4 \times 10^{-4}$, so $L \ll 1$ and Equation (S.11) is valid.

Conversion of terahertz transmission data to photoconductivity

This section outlines how photoconductivity $\Delta\sigma$ is extracted from our OPTP measurement of $\frac{\Delta E}{E}$.

Using SEM images of nanowires on quartz, we calculated the effective areal fill factor of nanowires, f_w, for each sample. We consider the nanowires to be embedded within the surrounding vacuum, within a layer of thickness δ. The transmitted terahertz electric fields with and without the optical pump are defined as

$$E_\mathrm{on} = f_\mathrm{w} E_{\mathrm{w}^*} + (1 - f_\mathrm{w}) E_\mathrm{v} \tag{S.13}$$

$$E_\mathrm{off} = f_\mathrm{w} E_\mathrm{w} + (1 - f_\mathrm{w}) E_\mathrm{v}, \tag{S.14}$$

where E_w and E_v are the terahertz transmission through the nanowires and the surrounding vacuum, respectively, and * indicates a photoexcited state. Note that the pump beam does not change the complex refractive index of the vacuum. The electric fields E_v, E_w and E_{w^*} may then be written as

$$E_\mathrm{v} = e^{i n_\mathrm{v} \omega \delta / c} E_\mathrm{i} \tag{S.15}$$

$$E_\mathrm{w} = t_\mathrm{vw} t_\mathrm{wv} e^{i n_\mathrm{w} \omega \delta / c} \mathrm{FP}_\mathrm{vwv} E_\mathrm{i} \tag{S.16}$$

$$E_{\mathrm{w}^*} = t_{\mathrm{vw}^*} t_{\mathrm{w}^*\mathrm{v}} e^{i n_{\mathrm{w}^*} \omega \delta / c} \mathrm{FP}_{\mathrm{vw}^*\mathrm{v}} E_\mathrm{i}, \tag{S.17}$$

where FP_{ijk} are the Fabry-Pérot terms, t_{ij} are the Fresnel transmission coefficients, c is the speed of light in vacuum, and n_{w^*} and n_{w} are the refractive indices of nanowires with and without photoexcitation, respectively.

Combining Equations (S.13) and (S.14) gives

$$\frac{E_{\mathrm{w}^*}}{E_{\mathrm{w}}} = \frac{\Delta E}{E}\left[1+\left(\frac{1}{f_{\mathrm{w}}}-1\right)\frac{E_{\mathrm{v}}}{E_{\mathrm{w}}}\right]+1, \tag{S.18}$$

where $\Delta E = E_{\mathrm{on}} - E_{\mathrm{off}}$. Note that the OPTP system gives direct experimental measurement of $\frac{\Delta E}{E}$ where ΔE is the photoinduced change in terahertz probe transmission and $E = E_{\mathrm{off}}$ is the terahertz probe transmission in the absence of photoexcitation.

At terahertz frequencies the thin film limit is valid because $\frac{n\omega\delta}{c} \ll 1$. In the thin film limit we can make the approximation $\frac{E_{\mathrm{v}}}{E_{\mathrm{w}}} = 1$. Using this approximation and rearranging Equation (S.18), we define parameter A as

$$A = \frac{E_{\mathrm{w}}}{E_{\mathrm{w}^*}} = \frac{1}{\frac{1}{f_{\mathrm{w}}}\frac{\Delta E}{E}+1}. \tag{S.19}$$

Substituting the appropriate forms of FP_{ijk} and t_{ij} into Equations (S.15) to (S.17) and applying the thin film limit $e^{in\omega\delta/c} = 1 + in\omega\delta/c$ gives

$$\frac{E_{\mathrm{w}^*}}{E_{\mathrm{w}}} = \frac{2-\frac{i\omega\delta}{c}(1+n_{\mathrm{w}}^2)}{2-\frac{i\omega\delta}{c}(1+n_{\mathrm{w}^*}^2)}, \tag{S.20}$$

The following general relations can then be substituted into Equation (S.20)

$$n_{\mathrm{w}}^2 = \varepsilon_{\mathrm{w}} \tag{S.21}$$

$$n_{\mathrm{w}^*}^2 = \varepsilon_{\mathrm{w}^*} \tag{S.22}$$

to give

$$\varepsilon_{w^*} = \left[-\frac{E_w}{E_{w^*}} \left(2\frac{c}{i\omega\delta} - (1+\varepsilon_w) \right) + 2\frac{c}{i\omega\delta} - 1 \right], \tag{S.23}$$

where ε_{w^*} and ε_w are the dielectric constants of the nanowires with and without photoexcitation, respectively. The photoinduced conductivity, $\Delta\sigma$, is given by

$$\varepsilon_{w^*} = \varepsilon_w + \frac{i\Delta\sigma}{\omega\varepsilon_0}, \tag{S.24}$$

where ε_0 is the permittivity of free space. Substituting Equation (S.23) into Equation (S.24) gives the following expression for $\Delta\sigma$ in terms of the measured signal $\frac{\Delta E}{E}$:

$$\Delta\sigma = \varepsilon_0 (A-1) \left[\frac{2c}{\delta} - i\omega (1+\varepsilon_w) \right], \tag{S.25}$$

where A is defined in Equation (S.19). Thus, using Equations (S.25) and (S.19), the measured signal can be converted to $\Delta\sigma$ using $\varepsilon_w = 12.5$ as for bulk InP and values of f_w and δ as measured from SEM images.

Spatial separation due to band-bending at nanowire surfaces

An alternative mechanism for spatial separation of electrons and holes concerns band bending at the nanowire surface. Band bending effects have been observed in semiconductor structures with high surface area-to-volume ratios such as p-type InP nanowires,[3] Ge nanowires[4] and porous InP.[5] In InP, surface states tend to pin the Fermi level within 0 to 0.34 eV of the conduction band edge, depending on the crystallographic orientation of the surface.[6,7] It is reasonable to assume that the nanowire side facets, which are predominantly $\{1\bar{1}00\}$ oriented, will experience surface Fermi level pinning near the conduction band edge. Assuming the InP is doped at $5.5 \times 10^{16}\,\mathrm{cm}^{-3}$ (as justified in the main manuscript), the Fermi level pinning creates band bending such that the electrons become confined to the surface and the holes to the centre of the nanowire. At early times after photoexcitation the carrier density would screen this surface field, reducing band bending and

increasing the likelihood of electron–hole recombination. Consequently, PL would be observed at early times. At later times, however, when the carrier density is lower, the surface field would result in spatial separation of electrons and holes, which would suppress radiative recombination and would account for the rapid quenching of PL at 1.43 eV.

A study by van Weert *et al.*, however, demonstrated that band-bending effects are only pronounced in p-InP nanowires.[3] The nanowires of our study are thought to be n-type, and exhibited a very low surface recombination velocity, indicating that band-bending effects are negligible. Therefore presence of stacking faults and ZB/WZ polytypism is more likely to account for our observations of a short PL lifetime coupled with a long photoconductivity lifetime.

Spatial separation due to ZB/WZ band offsets

In WZ InP, the conduction band is approximately 129 meV higher in energy, and the valence band is approximately 45 meV higher in energy, than in ZB InP. ZB sections within a nanowire are therefore potential wells for electrons, whereas WZ sections are potential wells for holes. Due to quantum confinement, electrons and holes occupy discrete energy levels within these wells, with the energy level depending on the thickness of the well. We calculated the eigenstates of finite square wells to determine these energy levels as a function of well thickness. As the WZ sections in these nanowires are typically thick, the hole states will lie at, or near the WZ valence band edge, 45 meV above the ZB valence band edge. This is significantly higher than the thermal energy at room temperature, $k_{\mathrm{B}}T = 26$ meV, so there should be little thermal excitation of holes out of the WZ potential wells. The ZB sections occur at higher densities at the nanowire bases, where they are typically 1 nm to 3 nm in width. For ZB wells 2 nm in width, the lowest lying energy state is 29 meV below the WZ conduction band edge. This is above the thermal energy at room temperature, $k_{\mathrm{B}}T = 26$ meV. Therefore, for ZB potential wells greater than 2 nm in thickness, there should be little thermal excitation of electrons at room temperature. For ZB sections less than 2 nm in thickness, however, the electrons are only weakly localized.

Photoexcited carrier density

The photoexcited carrier density, N_{p}, within a sample of thickness d is given by

$$N_{\mathrm{p}} = \frac{I}{Ed}\left(1 - e^{-d/\alpha}\right), \tag{S.26}$$

where I is the photoexcitation fluence, α is the absorption depth and E is the photon energy. At our photoexcitation wavelength of $\lambda = 800\,\mathrm{nm}$, $\alpha = 400\,\mathrm{nm}$ for InP. This α is significantly larger than all the nanowire diameters we studied, which places the nanowires in the thin film limit. This means that for a given photoexcitation intensity, the photoexcited carrier density is approximately constant regardless of nanowire diameter.

Fluence dependence of photoconductivity decay rate

Figure S.3 shows the decays of $\Delta E/E$ with time after photoexcitation for two different InP nanowire samples: 50 nm diameter and 135 nm diameter. From Figure S.3 it is evident that the decay lifetime is approximately constant at all photoexcitation fluences. Similarly, the other two samples, of 85 nm and 160 nm diameter, showed constant decay lifetimes regardless of photoexcitation fluence. This indicates that the carrier lifetime is minimally affected by the carrier density.

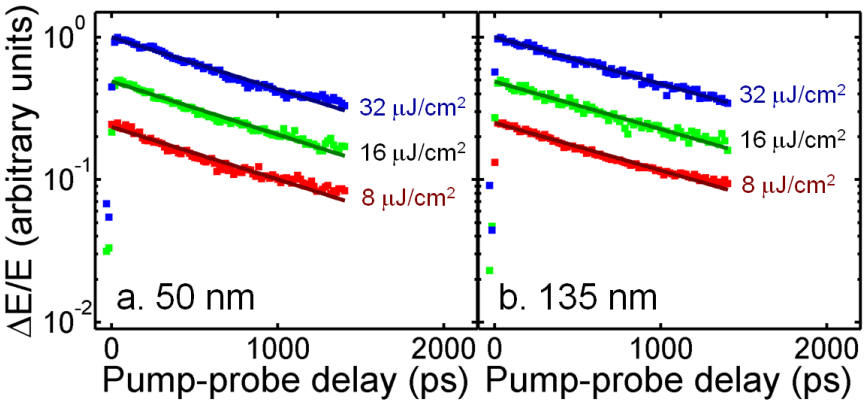

Figure S.3: Pump-induced change in terahertz electric field ($\Delta E/E$) at different pump–probe delays, for (a) 50 nm and (b) 135 nm diameter InP nanowires. Results for three different photoexcitation fluences are plotted: 8, 16 and 32 μJ/cm^2.

Calculation of theoretical scattering rates in bulk InP

Theoretical scattering rates for bulk InP are plotted in the dotted curve of Figure 4g. These scattering rates were calculated assuming parameters for bulk ZB InP, such as phonon frequency and $m_e^* = 0.08m_e$. Electron–phonon, electron–electron, electron–hole and electron–plasmon mechanisms were included in the rates. The calculation follows published models.[8,9] Carrier distributions were assumed to be thermalised and at room temperature. An ionised donor density of $5.5 \times 10^{16}\,\mathrm{cm}^{-3}$ was assumed for calculation of electron–impurity scattering. Electron–phonon scattering dominates the calculated scattering rates at low carrier density and is roughly independent of carrier density. The rates for electron–electron, electron–hole and electron–plasmon scattering increase with carrier density.

Photoconductivity spectral evolution

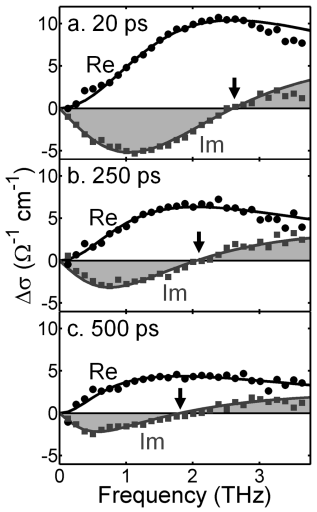

Figure S.4: Time-resolved conductivity of photoexcited carriers in 50 nm InP nanowires at times (a) 20 ps, (b) 250 ps and (c) 500 ps after the pump excitation pulse. The symbols are the measured data and the lines are the fitted plasmon responses. The real (circles and lines) and imaginary (squares and lines) components of the conductivity are plotted. The incident pump pulse fluence was $10\,\mu\mathrm{J/cm}^2$. The arrow indicates the resonant surface plasmon frequency ω_0.

Figure S.4 shows photoconductivity spectra of 50 nm nanowires taken various times after pho-

toexcitation. The surface plasmon resonance shifts to lower frequencies with time, reflecting the decay in carrier density with time.

Photoconductivity spectra of nanowires of different diameter

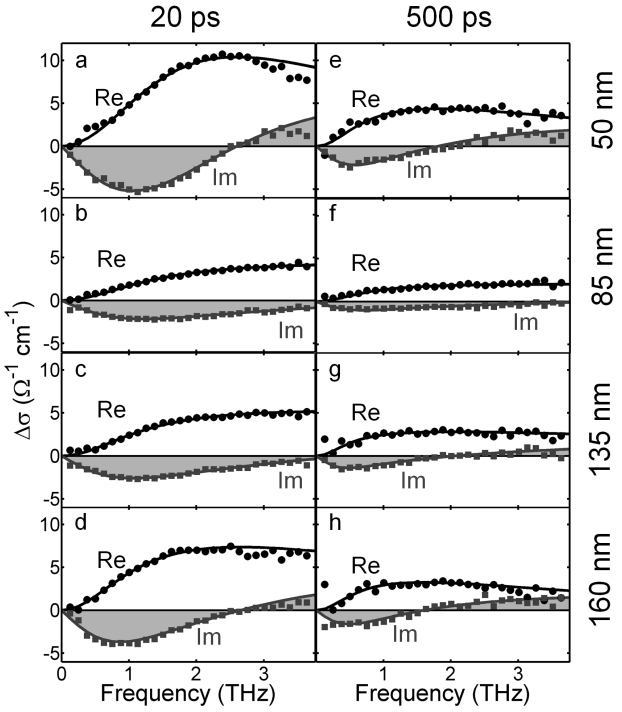

Figure S.5: Conductivity of photoexcited carriers in (a, e) 50, (b, f) 85, (c, g) 135 and (d, h) 160 nm diameter InP nanowires at (a-d) 20 ps after photoexcitation and (e-h) 500 ps after photoexcitation with a pump pulse of fluence 10 μJ/cm^2. The symbols are the measured data and the lines are the fitted plasmon responses. The real (circles and lines) and imaginary (squares and lines) components of the conductivity are plotted.

Figure S.5 shows photoconductivity spectra taken for the four different nanowire samples of 50, 85, 135 and 160 nm diameter. These spectra were measured at 20 ps and 500 ps after photoexcitation with a pump fluence of 10 μJ/cm^2. The extracted scattering rates and mobilities are summarized in Table S.1. After photoexcitation, the photoexcited carrier density decays. As the photoexcited carrier density decays, the scattering rate exhibits a small decrease, because carrier–carrier scattering decreases.

At 20 ps after photoexcitation, the extracted scattering rates were 3.3×10^{13} s^{-1}, 18×10^{13} s^{-1},

$10 \times 10^{13}\,\mathrm{s}^{-1}$ and $4.5 \times 10^{13}\,\mathrm{s}^{-1}$ respectively for the 50, 85, 135 and 160 nm diameter nanowires. These scattering rates correspond to mobilities of 660, 120, 220 and 480 $\mathrm{cm}^2\mathrm{V}^{-1}\mathrm{s}^{-1}$. In the data of Table S.1, we observe only a weak dependence of mobility on time after photoexcitation. Therefore these mobility values are valid for a wide range of carrier densities.

Table S.1: Electron scattering rates (γ) and mobilities (μ) extracted from the spectra of Figure S.5 for the four nanowire samples of different diameter (d).

Diameter, d (nm)	Pump–probe delay (ps)	γ (s^{-1})	μ ($\mathrm{cm}^2\mathrm{V}^{-1}\mathrm{s}^{-1}$)
50 nm	20 ps	3.3×10^{13}	660
	500 ps	3.1×10^{13}	700
85 nm	20 ps	18×10^{13}	120
	500 ps	17×10^{13}	130
135 nm	20 ps	10×10^{13}	220
	500 ps	9.0×10^{13}	260
160 nm	20 ps	4.5×10^{13}	480
	500 ps	4.2×10^{13}	530

Transport parameters for InP nanowires

Table S.2 summarises the transport parameters extracted from the OPTP measurements on the four samples of 50, 85, 135 and 160 nm diameter. The photoexcited carrier lifetime, τ, was inferred from the photoconductivity decays of Figure 2a. The electron scattering rate, γ, was extracted from the spectra of Figure S.5. Using τ and γ, quantities for the electron mobility (μ), mean free path (λ), diffusion constant (D) and diffusion length (L) were calculated using

$$\mu = \frac{e}{m_{\mathrm{e}}^{*}\gamma} \tag{S.27}$$

$$\lambda = v\tau \tag{S.28}$$

$$D = \frac{\mu k_{\mathrm{B}} T}{e} \tag{S.29}$$

$$L = \sqrt{D\tau} \tag{S.30}$$

where e is the electronic charge, m_e^* is the electron effective mass, v is the electron thermal velocity at room temperature and k_B is the Boltzmann constant. We deduce v by solving the equation

$$E = \frac{1}{2} m_e^* v^2 = \frac{3}{2} k_B T \tag{S.31}$$

to give $v = 4.1 \times 10^5\ \mathrm{ms}^{-1}$.

Table S.2: Parameters extracted for the four nanowire samples of different diameter (d), including photoexcited carrier lifetime (τ), electron scattering rate (γ), electron mobility (μ), mean free path (λ), diffusion constant (D) and diffusion length (L).

d (nm)	τ (ns)	γ (s^{-1})	μ ($cm^2V^{-1}s^{-1}$)	λ (nm)	D (cm^2s^{-1})	L (nm)
50	1.18	3.3×10^{13}	660	12	17	1400
85	1.27	18×10^{13}	120	2.3	3.1	630
135	1.30	10×10^{13}	220	4.1	5.7	860
160	1.34	4.5×10^{13}	480	9.1	13	1300

References

(1) Léonard, F.; Talin, A. A.; Swartzentruber, B. S.; Picraux, S. T. *Phys. Rev. Lett.* **2009**, *102*, 106805.

(2) Dan, Y.; Seo, K.; Takei, K.; Meza, J. H.; Javey, A.; Crozier, K. B. *Nano Lett.* **2011**, *11*, 2527–2532.

(3) van Weert, M. H. M.; Wunnicke, O.; Roest, A. L.; Eijkemans, T. J.; Silov, A. Y.; Haverkort, J. E. M.; 't Hooft, G. W.; Bakkers, E. P. A. M. *Appl. Phys. Lett.* **2006**, *88*, 043109.

(4) Prasankumar, R. P.; Choi, S.; Trugman, S. A.; Picraux, S. T.; Taylor, A. J. *Nano Lett.* **2008**, *8*, 1619–1624.

(5) Lloyd-Hughes, J.; Mueller, S.; Scalari, G.; Bishop, H.; Crossley, A.; Enachi, M.; Sirbu, L.; Tiginyanu, I. M. *Appl. Phys. Lett.* **2012**, *100*, 132106.

(6) Koenders, L.; Bartels, F.; Ullrich, H.; Monch, W. *J. Vac. Sci. Technol. B* **1985**, *3*, 1107–1115.

(7) Moison, J. M.; Bensoussan, M. *Surf. Sci.* **1986**, *168*, 68–73.

(8) Yu, P. Y.; Cardona, M. *Fundamentals of Semiconductors*, 3rd ed.; Springer, Berlin, 2005.

(9) Lloyd-Hughes, J. *Appl. Phys. Lett.* **2012**, *100*, 122103.